Computers and Concrete, *Vol. 12, No. 4 (2013) 565-583*
DOI: http://dx.doi.org/10.12989/cac.2013.12.4.565

On modeling coupling beams incorporating strain-hardening cement-based composites

Chung-Chan Hung* and Yen-Fang Su

Civil Engineering, National Central University, Taoyuan County, 32011,Taiwan

(Received February 20, 2013, Revised May 26, 2013, Accepted June 6, 2013)

Abstract. Existing numerical models for strain-hardening cement-based composites (SHCC) are short of providing sufficiently accurate solutions to the failure patterns of coupling beams of different designs. The objective of this study is to develop an effective model that is capable of simulating the nonlinear behavior of SHCC coupling beams subjected to cyclic loading. The beam model proposed in this study is a macro-scale plane stress model. The effects of cracks on the macro-scale behavior of SHCC coupling beams are smeared in an anisotropic model. In particular, the influence of the defined crack orientations on the simulation accuracy is explored. Extensive experimental data from coupling beams with different failure patterns are employed to evaluate the validity of the proposed SHCC coupling beam models. The results show that the use of the suggested shear stiffness retention factor for damaged SHCC coupling beams is able to effectively enhance the simulation accuracy, especially for shear-critical SHCC coupling beams. In addition, the definition of crack orientation for damaged coupling beams is found to be a critical factor influencing the simulation accuracy.

Keywords: strain-hardening cement-based composites; coupling beams; numerical modeling; cyclic loading; hysteretic responses; crack patterns

1. Introduction

Reinforced concrete (RC) coupled wall systems are often used to provide strength and stiffness to resist lateral forces in medium- to high-rise structural systems. A coupled wall system consists of two or more shear walls connected by coupling beams as shown in Fig. 1. The coupling action induced by the coupling beams is shown to be able to reduce the demand for flexural stiffness and strength from the individual walls. The coupling beams are expected to provide sufficient strength, ductility, and energy dissipation capacity under seismic actions. If the coupling beams are significantly damaged and lose their ability to sustain shear forces, the coupled walls will no longer act as an integrated system and will behave like individual shear walls, leading to a substantially magnified wall response.

In order to achieve a sufficient capacity, a dense array of shear reinforcement and confinement is required in RC coupling beams. The 2011 ACI Building code (2011) requires the use of heavily confined diagonal reinforcement cages for short and highly stressed RC coupling beams. The use

*Corresponding author, Assistant Professor, Ph.D., E-mail: cchung@ncu.edu.tw

http://www.techno-press.org/?journal=cac&subpage=8 ISSN: 1598-8198(Print), 1598-818X (Online)

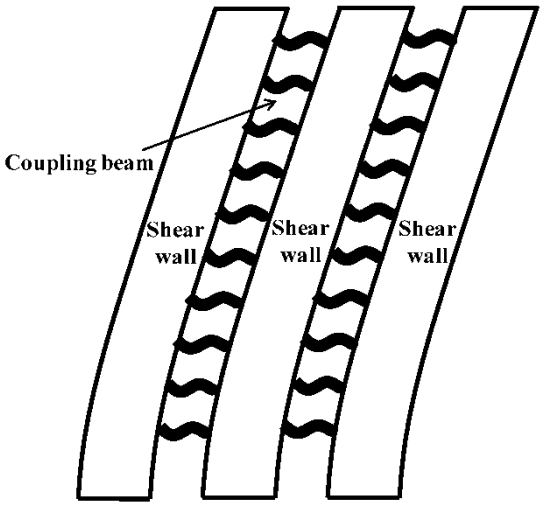

Fig. 1 Coupled wall system

of diagonal reinforcement cages not only increases the ductility and stiffness retention of coupling beams, but also eliminates the development of sliding shear failures. Nevertheless, the strict requirements for the reinforcement detailing significantly reduces the constructability of RC coupling beams. In addition, the dense array of reinforcement required for coupling beams may interfere with reinforcement in the wall boundary elements.

Strain-hardening cement-based composites (SHCC) are a class of cementitious materials that possesses significantly enhanced behavior over traditional concrete as shown in Fig. 2. When SHCC is subjected to tensile force, it initially exhibits a similar elastic behavior to that of regular concrete. Nevertheless, while regular concrete fails immediately after the first crack occurs, SHCC shows a unique strain hardening behavior accompanied by multiple hairline cracks. After that, further deformation demands are gradually accommodated within a single growing crack or band of cracks (Kim *et al*. 2009) , which typically occurs at strains ranging between 0.5% and 4% (about 2 orders of magnitude greater than traditional concrete). The unique tensile behavior of the material level transfers into the enhanced ductility, shear resistance, damage tolerance, and energy dissipation capacity in the structural level (Kesner and Billington 2005, Lequesne *et al*. 2009, Esmaeeli *et al*. 2013, Hung and El-Tawil 2011, Mechtcherine 2013). In compression (Fig. 2(b)), SHCC behave like confined concrete, i.e. the material has greater strength and ductility compared to regular concrete. In recent years, researchers have begun exploring the potential benefits of the incorporation of HPRFC in coupling beams. Studies (Lequesne *et al*. 2010) suggest that using SHCC to replace regular concrete in coupling beams will simplify the process of reinforcement detailing and reduce the amount of reinforcement required while still ensuring stable hysteresis behavior. It has also been shown that the ductility and energy dissipation capacity of the SHCC coupling beam can be substantially enhanced compared to those of traditional RC coupling beams.

Although there is experimental evidence of the attractive performance of SHCC coupling beams in the component scale, efforts are still needed to investigate the impact of SHCC coupling beams on the performance of large scale coupled wall systems. It is, however, difficult to conduct experimental investigations due to the fact that a large scale coupled wall system is costly to build

and difficult to test. On the other hand, there are no existing numerical models that are robust and accurate enough in modeling the detailed hysteretic behavior and crack patterns of SHCC coupling beams. The objective of the presented study is to develop a reliable and accurate computational model to simulate the complex cyclic behavior of SHCC coupling beams. For this purpose, various SHCC coupling beam models based on the smeared crack approach are proposed. The performance of each model is demonstrated by comparing the predicted solutions with the experimental results from a series of cyclic loading tests on SHCC coupling beams with different span length-to-depth ratios (aspect ratios). Valuable insights into the applicability of each model are obtained. The most accurate and reliable modeling scheme is suggested based on the comparison results.

2. Modeling methodology

2.1 Crack modeling

Two approaches are often employed in order to model the effect of cracks on the behavior of regular concrete materials, i.e., the discrete crack approach and the smeared crack approach. In the former it is assumed that a crack occurs as soon as the nodal force exceeds the prescribed tensile strength. The crack is presented using a geometrical discontinuity between the original node and the newly formed node. The development of the remeshing technique and crack elements has further advanced the discrete crack approach (De Borst 1997). Nevertheless, its high demand for computational resources makes it impractical for large-scale structure modeling. In contrast, the smeared crack approach assumes that cracks exist in a uniformly continuous sense (Kim *et al*. 2012; Vecchio and Minelli 2006, Hung *et al*. 2013). In the smeared crack approach, crack initiation is defined using a strain criterion. It is assumed that a crack will be initiated when the principal strain at a certain integration point reaches the prescribed cracking strain. The effect of cracks on the concrete behavior is addressed by directly modifying the material stress-strain relationship. An important advantage of the smeared crack approach is that it only requires limited computational effort to model the detailed concrete cyclic behavior. The ability of being able to reproduce the experimentally observed stress-strain relationships also contributes to the popularity of this approach. The smeared crack approach is therefore employed to model the SHCC coupling beams in this study. In addition, the co-rotational scheme (Kwan and Bllington 2001), which allows the development of a pair of orthogonal cracks at an integration point, is employed to model the influence of cracks on the cyclic response of SHCC coupling beams.

2.2 Crack orientation

The rotating crack model (Hung and Li 2013) and the fixed crack model (Said *et al*. 2005) are often used to define crack orientations for brittle concrete materials. The former assumes that the crack plane continues to rotate after initiating, whereas the latter fixes the crack plane as soon as a crack occurs. Past research has shown that both models have attained varying degrees of success for modeling brittle cement-based materials (De Borst 1997). However, their feasibility for simulating the behavior of SHCC that shows a different failure pattern than regular concrete remains to be explored. In this study, the applicability of these two models for SHCC coupling beams is assessed. Additionally, in order to account for the enhanced damage tolerance and crack

patterns of the SHCC over brittle concrete materials, a modified fixed crack method is introduced (Hung and El-Tawil 2010). In comparison with the traditional fixed crack approach, the modified fixed crack method allows a crack plane to continuously rotate until crack localization occurs. In other words, the multiple narrow cracks associated with the tensile strain hardening behavior are assumed to be temporary damage in the modified fixed crack model. Only the localized cracks that cause material softening behavior are regarded as permanent damage.

2.3 SHCC constitutive model

The SHCC constitutive model used in this study is based on total strain. The constitutive model is established according to the experimental observations from the uniaxial loading test on SHCC (Han *et al*. 2003). In the constitutive model, the current stress state is evaluated as a function of the current strain state and history parameters.

When SHCC is subjected to monotonic tensile loading, its behavior is assumed to consist of three linear segments as shown in Fig. 2(a), namely the elastic, the strain hardening, and the strain softening stages. The failure envelope in tension can be expressed as

$$\sigma = \begin{cases} \dfrac{\varepsilon}{\varepsilon_{tc}}\sigma_{tc} & for \quad 0 \le \varepsilon < \varepsilon_{tc} \\ \sigma_{tc} + \left(\sigma_{tp} - \sigma_{tc}\right)\left(\dfrac{\varepsilon - \varepsilon_{tc}}{\varepsilon_{tp} - \varepsilon_{tc}}\right) & for \quad \varepsilon_{tc} \le \varepsilon < \varepsilon_{tp} \\ \sigma_{tp}\left(1 - \dfrac{\varepsilon - \varepsilon_{tp}}{\varepsilon_{tu} - \varepsilon_{tp}}\right) & for \quad \varepsilon_{tp} \le \varepsilon < \varepsilon_{tu} \\ 0 & for \quad \varepsilon_{tu} \le \varepsilon \end{cases} \tag{1}$$

The monotonic compressive behavior of SHCC materials is also assumed to be composed of three stages: 1) a hardening behavior portion that is simulated by the Hognestad's parabolic function (Hung and Li 2013), 2) a linear softening portion, and 3) the stress plateau that represents the residual stress. The overall envelope for the monotonic compressive behavior, depicted in Fig. 2(b), can be expressed as

$$\sigma = \begin{cases} f'_{cc}\left[2\left(\dfrac{\varepsilon}{\varepsilon_{cp}}\right) - \left(\dfrac{\varepsilon}{\varepsilon_{cp}}\right)^2\right] & for \quad \varepsilon_{cp} \le \varepsilon < 0 \\ \sigma_{cp}\left(1 - \dfrac{\varepsilon - \varepsilon_{cp}}{\varepsilon_{cu} - \varepsilon_{cp}}\right) & for \quad \varepsilon_{cu} \le \varepsilon < \varepsilon_{cp} \\ k_0 f'_{cc} & for \quad \varepsilon \le \varepsilon_{cu} \end{cases} \tag{2}$$

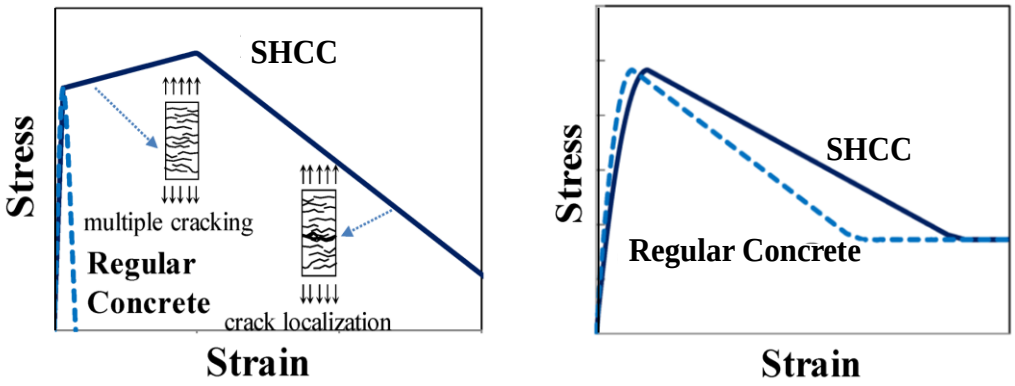

(a) tensile response (b) compressive response

Fig. 2 Typical monotonic behavior of SHCC

when SHCC is under cyclic tensile loading, the general stress-strain relationship can be idealized as

$$\sigma = \begin{cases} \dfrac{\varepsilon}{\varepsilon_{tc}}\sigma_{tc} & for \quad 0 \le \varepsilon_{t\max} < \varepsilon_{cp} \\ \max\left\{0, \sigma^*_{t\min}\left(\dfrac{\varepsilon-\varepsilon_{tul}}{\varepsilon^*_{t\max}-\varepsilon_{tul}}\right)^{\alpha_t}\right\} & for \quad \varepsilon_{tc} \le \varepsilon_{t\max} < \varepsilon_{tp}, \dot{\varepsilon} < 0 \\ \min\left\{0, \sigma^*_{tul} + \left(\sigma_{t\max} - \sigma^*_{tul}\right)\left(\dfrac{\varepsilon-\varepsilon^*_{tul}}{\varepsilon^*_{t\max}-\varepsilon^*_{tul}}\right)\right\} & for \quad \varepsilon_{tc} \le \varepsilon_{t\max} < \varepsilon_{tp}, \dot{\varepsilon} \ge 0 \\ \max\left\{0, \sigma^*_{t\max}\left(\dfrac{\varepsilon-\varepsilon_{tul}}{\varepsilon^*_{t\max}-\varepsilon_{tul}}\right)\right\} & for \quad \varepsilon_{tp} \le \varepsilon_{t\max} < \varepsilon_{tu} \\ 0 & for \quad \varepsilon_{tu} \le \varepsilon_{t\max} \end{cases} \tag{3}$$

where $\varepsilon^*_{t\max} = \varepsilon_{t\max}$ for initial unloading; $\varepsilon^*_{t\max} = \varepsilon_{tprl}$ for unloading followed by partial reloading; $\varepsilon^*_{tul} = \varepsilon_{tul} = \beta_t \varepsilon_{t\max}$ for initial unloading; β_t is a constant for tensile unloading curve; $\varepsilon^*_{tul} = \varepsilon_{tpul}$ for unloading followed by partial reloading. In particular, when SHCC is under tension and unloading occurs, the unloading stress is expressed as an interpolation function between the two strain-stress states of $\left(\varepsilon^*_{t\max}, \sigma^*_{t\max}\right)$ and $\left(\varepsilon^*_{tul}, 0\right)$ in a power of α_t. When SHCC is under tension and reloading occurs, the stress state is linearly interpolated using the strain-stress states of $\left(\varepsilon^*_{tul}, \sigma^*_{tul}\right)$ and $\left(\varepsilon^*_{t\max}, \sigma^*_{t\max}\right)$. When SHCC materials are under random cyclic displacements in compression, the stress state can be calculated using

$$\sigma = \begin{cases} f'_{cc}\left[2\left(\dfrac{\varepsilon}{\varepsilon_{cp}}\right)-\left(\dfrac{\varepsilon}{\varepsilon_{cp}}\right)^2\right] & \text{for} \quad \varepsilon_{cp} \le \varepsilon_{c\min} < 0 \\ \min\left\{0, \sigma^*_{c\min}\left(\dfrac{\varepsilon-\varepsilon_{cul}}{\varepsilon^*_{c\min}-\varepsilon_{cul}}\right)^{\alpha_c}\right\} & \text{for} \quad \varepsilon_{cu} \le \varepsilon_{c\min} < \varepsilon_{cp},\ \dot{\varepsilon} > 0 \\ \min\left\{0, \sigma^*_{cul}+\left(\sigma_{c\min}-\sigma^*_{cul}\right)\left(\dfrac{\varepsilon-\varepsilon^*_{cul}}{\varepsilon_{c\min}-\varepsilon^*_{cul}}\right)\right\} & \text{for} \quad \varepsilon_{cu} \le \varepsilon_{c\min} < \varepsilon_{cp},\ \dot{\varepsilon} \le 0 \\ 0 & \text{for} \quad \varepsilon_{c\min} \le \varepsilon_{cu} \end{cases} \tag{4}$$

where $\varepsilon^*_{c\min} = \varepsilon_{c\min}$ for initial unloading conditions; $\varepsilon^*_{c\min} = \varepsilon_{cprl}$ for unloading conditions followed by partial reloading; $\varepsilon^*_{cul} = \varepsilon_{cul} = \beta_c \varepsilon_{c\min}$ for initial unloading conditions; β_c is a constant for compressive unloading curve; $\varepsilon^*_{cul} = \varepsilon_{cpul}$ for unloading followed by partial reloading. When SHCC is under compression and unloading occurs, the stress state is computed using an interpolation function between the strain-stress states of $\left(\varepsilon^*_{c\min}, \sigma^*_{c\min}\right)$ and $\left(\varepsilon^*_{cul}, 0\right)$ in a power of α_c. When SHCC is under compression and reloading occurs, the stress is evaluated using linearly interpolation with the strain-stress states of $\left(\varepsilon^*_{cul}, \sigma^*_{cul}\right)$ and $\left(\varepsilon^*_{c\min}, \sigma^*_{c\min}\right)$.

2.4 Model implementation

The implementation procedures for the three models are illustrated in Fig. 3. In the rotating crack scheme, the plane of the principal strain can be determined from the global strains using

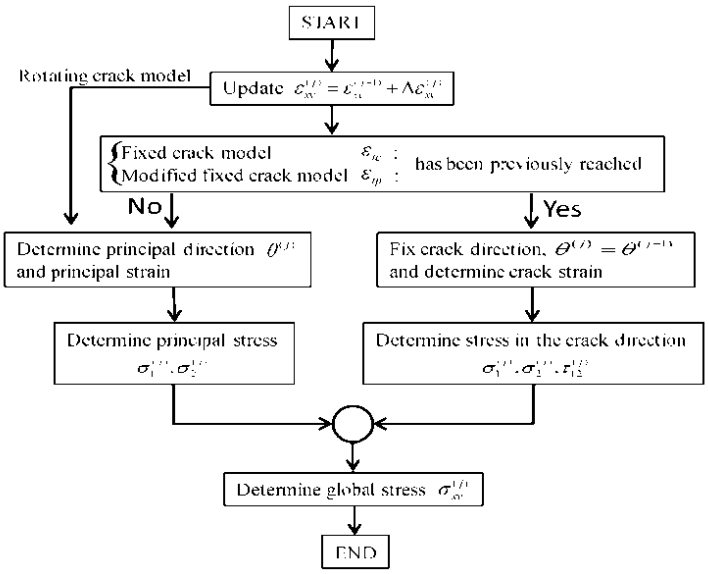

Fig. 3 Implementation procedures for the various smeared crack schemes

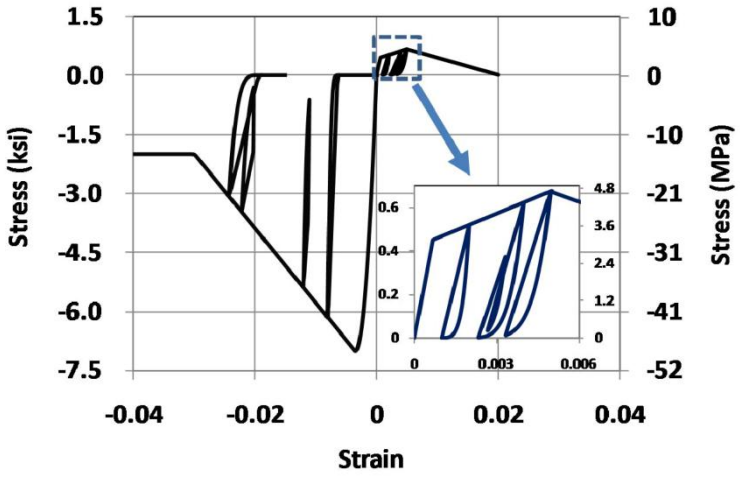

Fig. 4 Reversed stress-strain relationships of the SHCC constitutive model

Fig. 5 Experimental setup of the coupling beam testing

Mohr's circle. After that, the principal stresses are computed using the principal strain and the SHCC constitutive model. The principal stresses and directions are then used to calculate global stresses via Mohr's circle. In the rotating crack approach, the crack orientation (principal direction) is updated in every computational step after the first crack initiates. On the other hand, in the fixed crack approach, once the local strain reaches the cracking strain, the crack orientation is fixed and used for the following analysis steps. In the modified fixed crack model, the crack orientation is allowed to rotate after cracking initiates but is fixed after the local strain reaches the crack localization strain (ε_{tp}). The established SHCC material models are implemented as 2-D, plane stress, user-defined material models in LS-DYNA (Livermore Software Technology Corporation 2007). The subroutine for the user-defined model is compiled and linked to the LS-DYNA executable file to create a new executable file that can accommodate SHCC material behavior. Fig.

4 demonstrates the established SHCC stress-strain relationships using a single element subjected to random cyclic loadings.

3. Coupling beam experimental program

Three SHCC coupling beams with aspect ratios = 3.3, 2.75, and 1.75 (Lequesne *et al*. 2010) were tested. These SHCC coupling beams featured simplified reinforcement detailing and reduced reinforcement amounts compared to traditional RC coupling beam design. In particular, a single layer consisting of four bent diagonal steel bars was employed to replace the heavily confined diagonal reinforcement cages that are often used in RC coupling beams. Both ends of each coupling beam were embedded into stiff RC blocks that simulated the wall boundary elements. The bottom concrete block was fixed to the strong floor. Lateral displacement reversals were applied on the top concrete block using hydraulic actuators. In order to simulate the shear walls with equal curvatures during seismic actions, two vertically pinned steel links were used to restrain the vertical displacement of the top concrete block during testing. A picture of the experimental setup for the coupling beams is shown in Fig. 5.

4. Cyclic behavior of the coupling beams

4.1 Coupling beam with an aspect ratio of 3.3 (CB33)

The first SHCC coupling beam had a cross section of $500mm \times 150mm$ and was 1650 mm in length. Four #6 (D20) were used for the diagonal reinforcement. Longitudinal reinforcement was placed in two identical layers, and each layer consisted of two #3 (D10) and two #6 (D20) bars. #4 (D12) stirrups with a spacing of 75 mm were placed at the boundary zone, and #3 (D10) stirrups with a spacing of 150 mm were in the middle portion of the beam. The reinforcement details are shown in Fig. 6(a). CB33 is numerically built using LS-DYNA based on the experimental program. The SHCC material is modeled using 2-D plane stress elements. The steel bars are represented using nonlinear truss elements. A perfect bond is assumed between the steel bars and the surrounding SHCC material. Material parameters for the SHCC constitutive models used throughout this study are listed in Table 1, and are chosen according to the average properties determined from experimental tests. Steel behavior is assumed to be elastic-plastic with kinematic hardening plasticity. The tensile stress-strain properties of the reinforcing steel are obtained by direct tensile tests and the results are listed in Table 2. The numerical coupling beam model is fixed at the bottom and restrained at the top in the vertical direction to simulate the physical boundary conditions. The developed numerical model for the CB33 is shown in Fig. 6(b).

The computed shear stress (normalized with respect to $\sqrt{f'_c}$) versus drift is plotted in Fig. 7. Fig. 7(a) shows the experimental results with the simulation solution obtained using the rotating crack model. It can be seen that the simulation solution is in good agreement with the experimental results in terms of the initial stiffness, stiffness retention, strength capacity, strength degradation, and pinching behavior. In the rotating crack model, a crack plane is in the direction of the principal plane, leading to a zero shear stress in the crack direction. In the fixed crack model, on the other hand, the direction of the principal plane does not necessarily coincide with the crack orientation.

The fixed crack model can therefore address the local shear resistance provided by aggregate interlock. Furthermore, in order to account for the reduced shear stiffness of damaged SHCC coupling beams, a retention factor is introduced in the fixed crack model. The retention factor is

Table 1 Material parameters for SHCC coupling beams

Material parameters	CB33	CB275	CB175
σ_{tc} (MPa)	4.1	4.1	2.8
ε_{tc}	0.00015	0.00015	0.00015
σ_{tp} (MPa)	5.2	5.2	3.5
ε_{tp}	0.004	0.004	0.004
ε_{tu}	0.17	0.17	0.17
σ_{cp} (MPa)	-61.4	-59.3	-41.4
ε_{cp}	-0.0035	-0.0035	-0.0025
σ_{cu} (MPa)	-20.7	-20.7	-13.8
ε_{cu}	-0.03	-0.03	-0.03
μ	0.2	0.2	0.2
p_1	0.0001	0.0001	0.0001
p_2	12	12	12
α_t	6	6	6
α_c	4	4	4
β_t	0.4	0.4	0.4
β_c	0.4	0.4	0.4

Table 2 Steel reinforcement properties (Lequesne *et al.* 2009, 2010)

	Bar size	Yield stress	Ultimate stress
CB275/CB33	#3 (D10)	370	604
	#4 (D13)	423	696
	#5 (D16)	421	683
	#6 (D19)	514	655
CB175	#3 (D10)	474	744
	#4 (D13)	438	686
	#5 (D16)	431	680

assumed as a function of the normal strain on the crack plane as illustrated in Fig. 8. As soon as cracking initiates, the shear stiffness is reduced to $G_i = \mu G_{SHCC}$; where $G_{SHCC} = \frac{E_{SHCC}}{2(1+v)}$; i

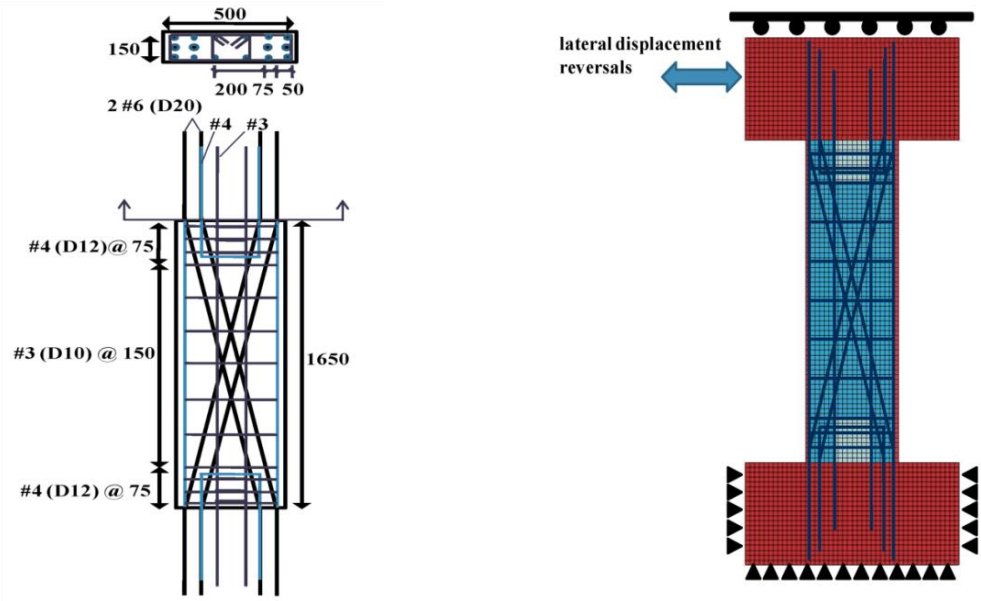

(a) reinforcing details (unit: mm) (b) numerical model

Fig. 6 Coupling beam with an aspect ratio of 3.3

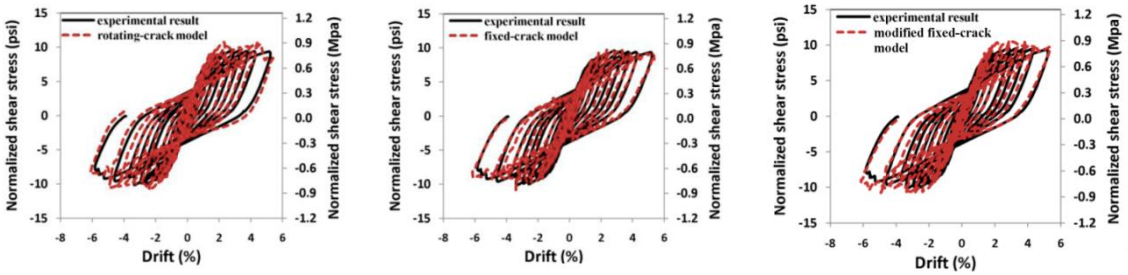

(a) rotating crack model (b) fixed crack model (c) modified fixed crack model

Fig. 7 Hysteresis behavior of the CB33

represents the direction, $i=1$ for crack direction, and $i=2$ for the direction normal to crack direction. As the normal strain continues to increase, the shear stiffness is assumed to decrease linearly. When the strain is larger than or equal to $\varepsilon_{\min}(=p_2\varepsilon_{tc})$, the retained shear modulus becomes a constant $G_{\min}=p_1G_{SHCC}$, where p_1 and p_2 are constants to define the minimum shear modulus and the corresponding strain, respectively. For regular concrete, Hassan (2004) suggested that the value of μ depends on the type of the simulated structure, while Sittipunt and Wood (1995) proposed that the general value of μ is 0.2. Based on calibration with the experimental data, a reasonable range of μ for SHCC coupling beams is found to be between 0.1 and 0.3. In particular, the calibration results show that when μ is larger than 0.3, the simulated results tend to underestimate the shear type of failure observed in the experimental program. When μ is less than 0.1, the coupling beam model is prone to premature failure. μ = 0.2 is used

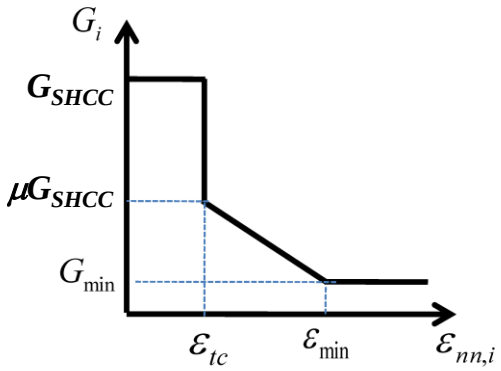

Fig. 8 Relationship between the normal strain and the shear stiffness for the fixed crack model

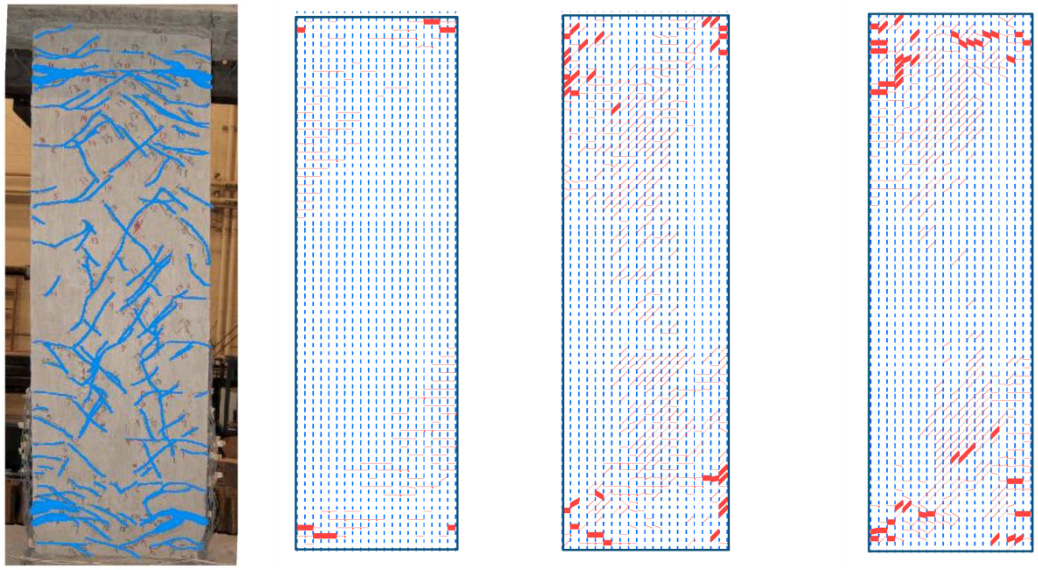

experimental result rotating crack model fixed crack model modified fixed crack model

Fig. 9 Relationship between the normal strain and the shear stiffness for the fixed crack model

throughout this study. The values of p_1 = 0.0001 and p_2 = 12 are decided based on the suggestions by Sittipunt and Wood (1995). In fact, it is found that when p_1 is less than 0.005, its variation has no obvious effects on the simulation results.

The predicted hysteresis behavior using the developed fixed crack model is plotted in Fig. 7(b). It can be seen that the performance of the fixed crack model is as good as that of the rotating crack model. In addition to the rotating crack model and fixed crack model, the modified fixed crack model is applied to predict the behavior of the CB33. As done in the fixed crack model, a shear stiffness retention factor is employed in the modified fixed crack model. Nevertheless, in the modified fixed crack model, the multiple narrow cracks that develop prior to crack localizations are assumed not to be significant enough to affect the shear modulus. The shear modulus is therefore not reduced until crack localization takes place. After crack localization occurs, the

retained shear modulus reduces linearly with the increased normal strain until the prescribed minimum shear modulus is reached. The hysteresis behavior of the CB33 simulated by the modified fixed crack model is shown in Fig. 7(c). It can be seen that the simulation solution catches the experimental results very well. Overall, all three schemes successfully simulate the hysteresis behavior of CB33, and the difference between each solution is negligible.

The performance of each model is further evaluated through the crack patterns of the CB33. The experimental result and the computed solutions are depicted in Fig. 9. The experimental results shown in Fig. 9(a) suggest that the failure pattern of CB33 was dominated by localized flexural cracks that developed at both ends of the specimen while narrow shear cracks were distributed throughout in the specimen. The solution using the rotating crack model is shown in Fig. 9(b). The thin lines denote fine cracking; localized cracks are represented by heavy lines; solid circles denote concrete crushing. Fig. 9(b) shows that the flexural failure pattern is successfully predicted by the rotating crack model. However, it underestimates the localized flexural cracks as well as the shear cracks. In contrast to the rotating crack model, both the fixed crack model and the modified fixed crack model capture the degree of localized flexural cracks with satisfactory accuracy as shown in Figs. 9(c)-(d). In addition, the observed narrow shear cracks in the experiment are reasonably simulated by both models. It is also noticed that all the numerical solutions show good agreement with the experimental results in that buckling is prevented in the diagonal steel bars by the confinement provided by SHCC.

4.2 Coupling beam with an aspect ratio of 2.75 (CB275)

The second coupling beam had an aspect ratio of 2.75 with dimensions of $1650mm \times 600mm \times 150mm\,(height \times span \times thickness)$. The reinforcement provided for the CB275 is shown in Fig. 10. The diagonal reinforcement consisted of four #6 (D20). Two #5 (D16) and two #3 (D10) were used in each layer of the flexural bars. #3 (D10) stirrups with a spacing of 200 mm and 75 mm were placed for the middle portion and boundary zone, respectively.

The computed normalized shear stress versus drift responses for the CB275 of the various numerical models are depicted in Fig. 11. As shown in Fig. 11(a), the rotating crack model significantly underestimates the pinching behavior and overrates the strength capacity of the CB275. Fig. 11(b) implies that the accuracy of computed pinching behavior and strength capacity are greatly improved by the fixed crack model. However, the pinching behavior remains underestimated and the strength degradation is not well captured by the fixed crack model. The simulation solution provided by the modified fixed crack model is plotted in Fig. 11(c). It can be seen that the simulation accuracy of the pinching behavior is further improved by the modified fixed crack model. The predicted shear stress capacity is approximately $0.9\sqrt{f'_c}\,(MPa)$, near 3.5%, matching the experimental results well. The strength degradation and stiffness retention are also simulated with reasonable accuracy by the modified fixed crack model.

The crack patterns from the experimental test and numerical modeling are depicted in Fig. 12. Experimental result (Fig. 12(a)) shows that the failure pattern of CB275 was dominated by the localized flexural cracks accompanied by a dense array of fine diagonal cracks. The crack pattern computed by the rotating crack model is plotted in Fig. 12(b). It can be seen that the rotating crack model overrates the degree of localized flexural cracks. It also significantly underestimates the development of shear cracks, leading to the much less pronounced pinching behavior in the

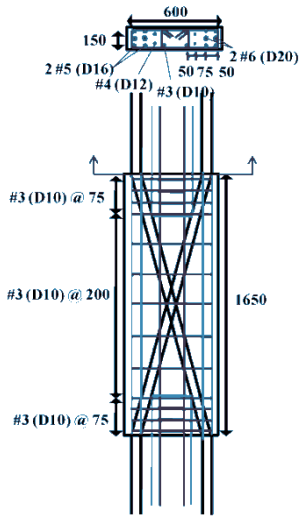

Fig. 10 Reinforcing details of the CB275 (unit: mm)

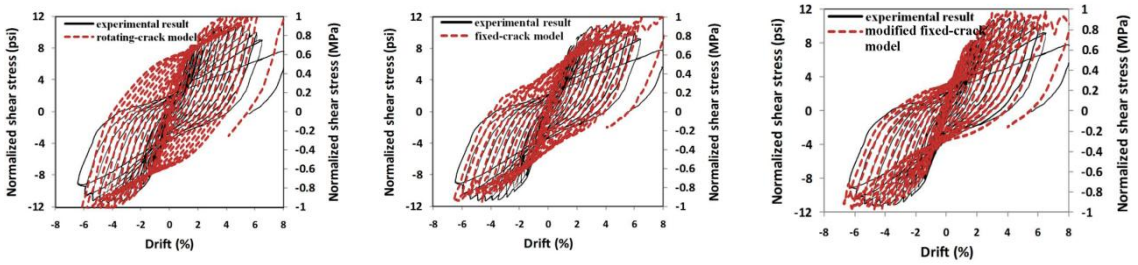

(a) rotating crack model (b) fixed crack model (c) modified fixed crack model

Fig. 11 Hysteresis behavior of the CB275

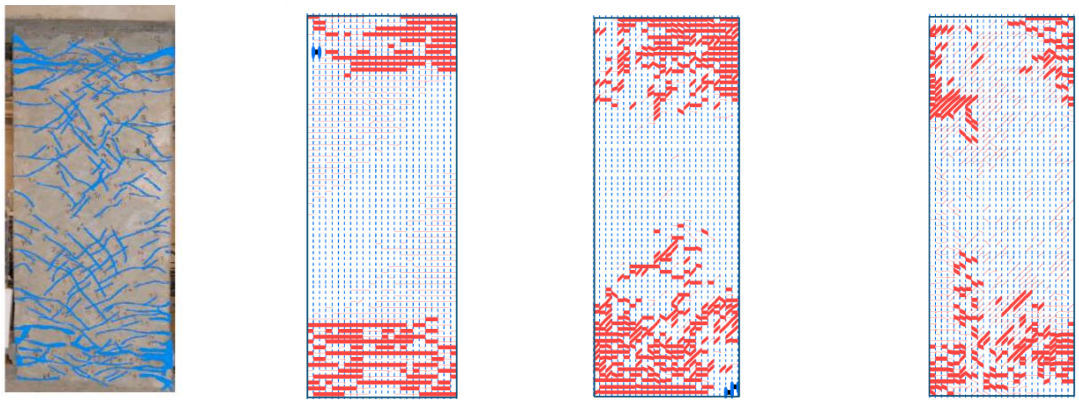

(a) experimental result (b) rotating crack model (c) fixed crack model (d) modified fixed crack model

Fig. 12 Crack patterns of the CB275

simulated hysteretic loops. Fig. 12(c) shows that the fixed crack model improves the simulation accuracy of the shear cracks. Nevertheless, the localized flexural cracks are slightly overestimated, causing the difference between the pinching behavior of the simulation solution and the experimental result. The computed crack patterns of the modified fixed crack model are depicted in Fig. 12(d). It shows that the degree of both localized flexural cracks and shear cracks are simulated with satisfactory accuracy. It is also noted that the computed localized damage distributes throughout the hinge region in the CB275, agreeing with the observation in the experimental test.

4.3 Coupling beam with an aspect ratio of 1.75 (CB175)

The third coupling beam had dimensions of $1050mm \times 600mm \times 150mm$ $(height \times span \times thickness)$ as shown in Fig. 13. The aspect ratio was 1.75. The diagonal reinforcement consisted of four #5 (D16). Two layers of flexural steel bars were employed, each layer consisting of two #4 (D12) and two #3 (D10). #3 (D10) stirrups with a spacing of 150 mm and 70 mm were used for the middle portion and boundary zone, respectively.

The hysteretic responses of the CB175 subjected to displacement reversals are shown in Fig. 14. It can be seen from Fig. 14(a) that the shear stress capacity is significantly overestimated by

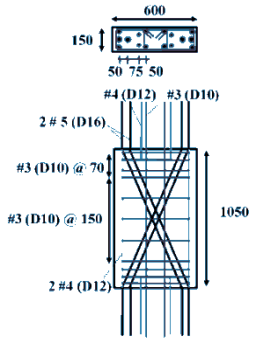

Fig. 13 Reinforcing details of the CB175 (unit: mm)

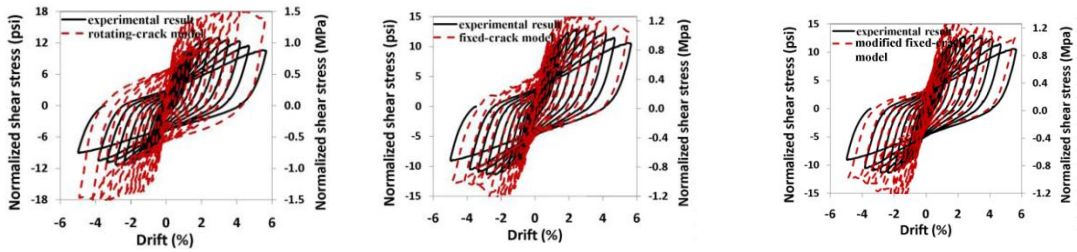

(a) rotating crack model (b) fixed crack model (c) modified fixed crack model

Fig. 14 Hysteresis behavior of the CB175

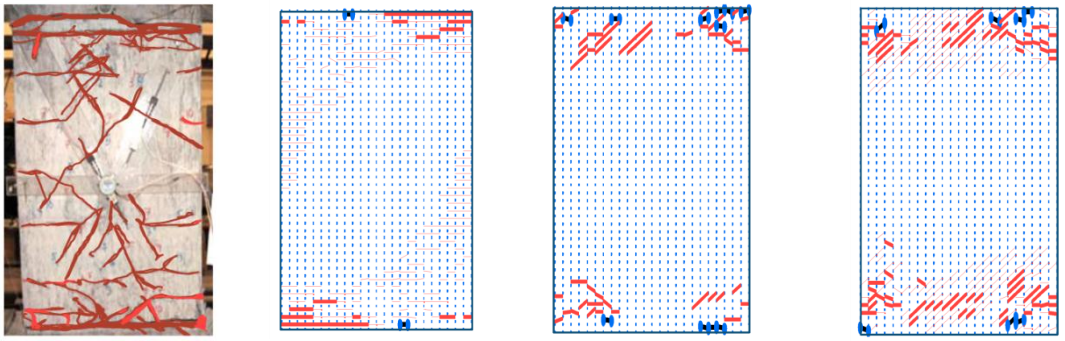

(a) experimental result (b) rotating crack model (c) fixed crack model (d) modified fixed crack model

Fig.15 Crack patterns of the CB175

the rotating crack model by nearly 50%. In addition, the pinching behavior and strength degradation are not well simulated. On the other hand, the fixed crack model and the modified fixed crack model substantially improve the simulation accuracy as shown in Figs. 14(b)-(c). Although the computed strength capacity is 20% larger than the experimental result, the pinching behavior, initial stiffness, strength degradation, and stiffness retention are simulated satisfactorily. It is noted that the simulated pinch behavior by the modified fixed crack model is slightly more pronounced than the experimental result in this case, while that given by the fixed model is more accurate. In general, the fixed crack model and modified fixed crack model achieve similarly good performance in the case of CB175.

The crack patterns are shown in Fig. 15. The experimental results shown in Fig. 15(a) suggest that the failure pattern of CB175 was dominated by widening flexural cracks accompanied by concrete crushing at both ends. Only scattered narrow diagonal cracks were present. Fig. 15(b) shows that the rotating crack model captures the flexural cracks and concrete crushing at both ends; however, it underestimates the shear cracks, as in previous examples. On the other hand, both the fixed crack model and modified fixed crack model successfully predict the presence of shear cracks, flexural cracks, and concrete crushing, as shown in Figs. 15(c) and 15(d). The computed dominating flexural cracks by both models are located near both ends, agreeing with the experimental observation and the intention of the detailing design (Lequesne *et al*. 2010). It is also noted that the modified fixed crack model predicts more shear cracks than the fixed crack model, leading to a slightly more pronounced pinching behavior (Fig. 14(c)).

5. Discussion

The evaluation examples show that all the numerical models are able to capture the stable hysteretic behavior of SHCC coupling beams subjected to cyclic loading. While the rotating crack model is able to model the flexural cracks, it substantially underestimates the shear cracks in all cases discussed. It is also shown that the rotating crack model is likely to cause an overestimated strength capacity of SHCC coupling beams. This tendency may have resulted from the assumption made in the rotating crack model that allows cracks to change directions. This assumption implies

that damage in concrete is temporary and violates the basic concept of permanency of damage in concrete members. In general, the fixed crack model with the shear retention factor is able to capture flexural and shear cracks and concrete crushing. Nevertheless, when it is applied to analyze shear-critical coupling beams, it slightly underestimates the shear cracks and pinching behavior. The simulation accuracy of the pinching behavior can be improved by the modified fixed crack model. The modified fixed crack model consistently captures the shear cracks with reasonable accuracy in all examples.

6. Conclusions

The evaluation examples show that all the numerical models are able to capture the stable hysteretic behavior of SHCC coupling beams subjected to cyclic loading. While the rotating crack model is able to model the flexural cracks, it substantially underestimates the shear cracks in all cases discussed. It is also shown that the rotating crack model is likely to cause an overestimated strength capacity of SHCC coupling beams. This tendency may have resulted from the assumption made in the rotating crack model that allows cracks to change directions. This assumption implies that damage in concrete is temporary and violates the basic concept of permanency of damage in concrete members. In general, the fixed crack model with the shear retention factor is able to capture flexural and shear cracks and concrete crushing. Nevertheless, when it is applied to analyze shear-critical coupling beams, it slightly underestimates the shear cracks and pinching behavior. The simulation accuracy of the pinching behavior can be improved by the modified fixed crack model. The modified fixed crack model consistently captures the shear cracks with reasonable accuracy in all examples.

Acknowledgements

The research described herein was sponsored in part by the National Science Council under Grant No. 101-2221-E-008-080. The authors would also like to acknowledge the assistance and ideas of Dr. Remy Lequesne and Ph.D. candidate Setkit Monthian at the University of Michigan, Ann Arbor. The opinions, findings, and conclusions expressed in this paper are those of the authors and do not necessarily reflect the views of the sponsor.

References

ACI (American Concrete Institute) Committee 318 (2011), ACI 318 Building Code Requirements for Structural Concrete, Farmington Hills, MI.

De Borst, R. (1997), "Some recent developments in computational modelling of concrete fracture", *Int. J. Fracture*, **86**(1-2), 5-36.

Han, T.S., Feenstra, P.H. and Billington, S.L. (2003), "Simulation of highly ductile fiber-reinforced cement-based composite components under cyclic loading", *ACI Struct. J.*, **100**(6), 749-757.

Hassan, M. (2004), *Inelastic Dynamic Behavior and Design of Hybrid Coupled Wall Systems*, Dissertation, Department of Civil and Environmental Engineering, University of Central Florida, FL.

Hung, C.C. and Li, S.H. (2013), "Three-dimensional model for analysis of high performance fiber reinforced cement-based composites", *Comp. Part B: Eng.*, **45**, 1441-1447.

Hung, C.C. and El-Tawil, S. (2011), "Seismic behavior of a coupled wall system with HPFRC materials in critical regions", *J. Struct. Eng. - ASCE*, **137**(2), 1395-1636.
Hung, C.C. and El-Tawil, S. (2010), "Hybrid rotating/fixed-crack model for high performance fiber reinforced cementitious composites", *ACI Mater. J.*, **107**(6), 569-577.
Hung, C.C. Su, Y.F. and Yu, K.H. (2013), "Modeling the shear hysteretic response for high performance fiber reinforced cementitious composites", *Constr. Build. Mater*., **41**, 37-48.
Kesner, K.E. and Billington, S.L. (2005), "Investigation of infill panels made from engineered cementitious composites for seismic strengthening and retrofit", *J. Struct. Eng. - ASCE*, **131**(11), 1712-1720.
Kim, D.J., El-Tawil, S. and Naaman, A.E. (2009), "Rate-dependent tensile behavior of high performance fiber reinforced cementitious composites", *Mater. Struct.*, **42**(3), 399-414.
Kim, K.S., Lee, D.H., Hwang, J.H. and Kuchma, D.A. (2012), "Shear behavior model for steel fiber-reinforced concrete members without transverse reinforcements ", *Comp. Part B: Eng.*, **43**, 2324-2334.
Kwan, W.P. and Billington, S.L. (2001), "Simulation of structural concrete under cyclic load", *J. Struct. Eng. - ASCE*, **127**(12), 1391-1401.
Lequesne, R.D., Parra-Montesinos, G.J. and Wight, J.K. (2009), "Test of a coupled wall with high-performance fiber-reinforced concrete coupling beams", *ACI SP265-01*, **265**, 1-18.
Lequesne, R.D., Setkit, M., Parra-Montesinos, G.J. and Wight, J.K. (2010), "Seismic detailing and behavior of coupling beams with high-performance fiber-reinforced concrete", *ACI SP271-11*, **272**, 189-204.
Livermore Software Technology Corporation. (2007), *LS-DYNA® Keyword User's Manual*.
Mechtcherine, V. (2013), "Novel cement-based composites for the strengthening and repair of concrete structures", *Constr. Build. Mater.*, **41**, 365-373.
Esmaeeli, E., Manning, E. and Barros, J.A.O. (2013), "Strain hardening fibre reinforced cement composites for the flexural strengthening of masonry elements of ancient structures", *Constr. Build. Mater.*, **38**, 1010-1021.
Said, A., Elmorsi, M. and Nehdi, M. (2005), "Non-linear model for reinforced concrete under cyclic loading", *Mag. Concrete Res.*, **57**(44), 211-224.
Sittipunt, C. and Wood, S.L. (1995), "Influence of web reinforcement on the cyclic response of structural walls", *ACI Struct. J.*, **92**(6), 745-756.
Vecchio, F.J. and Minelli F. (2006), "Compression field modeling of fiber-reinforced concrete members under shear loading", *ACI Struct. J.*, **103**(2), 244-252.

Notation

i	=	Direction
j	=	time step
μ	=	retention factor
$\theta^{(j)}$	=	angle of the principle/crack plane
f'_{cc}	=	compressive strength of SHCC adjusted to account for confinement effects
k_0	=	ratio of residual compressive stress to f'_{cc}
α_t	=	power for tensile unloading curve
α_c	=	power for compressive unloading curve
β_t	=	constant for tensile unloading curve
β_c	=	constant for compressive unloading curve
p_1	=	constant associated with the minimum shear modulus
p_2	=	constant associated with $\varepsilon_{\min}$
ν	=	Poisson's ratio
E_{SHCC}	=	Young's modulus
$G_{\min}$	=	minimum shear stiffness
G_{SHCC}	=	shear stiffness of the intact SHCC
G_i	=	shear stiffness in direction i
$\tau_{12}^{(j)}$	=	shear stress in local coordinate system
σ	=	Stress
$\sigma_1^{(j)}$	=	1st principal stress
$\sigma_2^{(j)}$	=	2nd principal stress
$\sigma_{xy}^{(j)}$	=	stress vector in global coordinate system
σ_{tc}	=	cracking stress
σ_{tp}	=	post-cracking stress
$\sigma^*_{t\min}$	=	minimum tensile stress for partial reloading
σ^*_{tul}	=	stress associated with ε^*_{tul}
$\sigma_{t\max}$	=	maximum experienced tensile stress
$\sigma^*_{t\max}$	=	maximum tensile stress for partial reloading
σ_{cp}	=	peak compressive stress
σ_{cu}	=	residual compressive stress
$\sigma^*_{c\min}$	=	minimum compressive stress for partial reloading
$\sigma_{c\min}$	=	minimum experienced compressive stress

σ^*_{cul}	=	stress associated with ε^*_{cul}
ε	=	Strain
$\dot{\varepsilon}$	=	strain rate
$\varepsilon_{\min}$	=	strain associated with $G_{\min}$
$\varepsilon_{nn,i}$	=	normal strain in direction i
$\varepsilon^{(j)}_{xy}$	=	strain vector in global coordinate system
ε_{tc}	=	cracking strain
ε_{tp}	=	post-cracking strain
ε_{tu}	=	ultimate tensile strain
ε_{tul}	=	minimum tensile strain during unloading
ε^*_{tul}	=	minimum tensile strain for partial reloading
$\varepsilon_{t\max}$	=	maximum experienced tensile strain
$\varepsilon^*_{t\max}$	=	maximum tensile strain for partial reloading
ε_{tprl}	=	maximum tensile strain during partial reloading
$\varepsilon_{c\min}$	=	minimum experienced compressive strain
$\varepsilon^*_{c\min}$	=	minimum compressive strain for partial reloading
ε_{cul}	=	maximum compressive strain during unloading
ε^*_{cul}	=	maximum compressive strain for partial reloading
ε_{cp}	=	peak compressive strain corresponding to f'_{cc}
ε_{cu}	=	ultimate compressive strain
ε_{cpul}	=	maximum compressive strain during partial unloading
ε_{cprl}	=	maximum compressive strain during partial reloading
$\Delta\varepsilon^{(j)}_{xy}$	=	incremental strain vector in global coordinate system
$\Delta\varepsilon^{(j)}_{y}$	=	incremental strain in y direction

CC